Megadrought: a series of unfortunate La Niña events?

Carlos M. Carrillo[1], Sloan Coats[2], Matt Newman[3,4], Dimitris A. Herrera[1], Xiaolu Li[1], Rick Moore[1], Sang-Ik Shin[3], Samantha Stevenson[5], Flavio Lehner[1,6], and Toby R. Ault[1]

[1]Earth and Atmospheric Sciences, Cornell University, Ithaca, New York, USA
[2]Department of Earth Sciences, University of Hawaii, Manoa, Hawaii, USA
[3]CIRES Climate Diagnostic Center, University of Colorado, Boulder, Colorado, USA
[4]Physical Sciences Division, NOAA/Earth System Research Laboratory, Boulder, Colorado, USA
[5]Bren School of Environmental Science & Management, University of California-Santa Barbara, Santa Barbara, California, USA
[6]Climate and Global Dynamics Laboratory, National Center for Atmospheric Research, Boulder, Colorado, USA

Version Dec 18, 2021

Corresponding author address: Dr. Carlos M. Carrillo, Earth and Atmospheric Sciences Department, Cornell University, 2140 Snee Hall, Ithaca, New York 14853. E-mail: carrillo@cornell.edu, phone: (607) 255-5173, fax: (607) 255-2106.

Key Points:

- In the US Southwest, megadroughts are not conditionally linked to low-frequency variability in the tropical Pacific.
- A hybrid modeling approach confirms the statistically significant occurrence of megadrought in the SWUS similar to paleoclimate records.
- A statistically plausible series of la Niña events may be sufficient to generate megadrought.

Abstract

Megadroughts are multidecadal periods of aridity more persistent than most droughts during the instrumental period. Paleoclimate evidence suggests that megadroughts occur in many parts of the world, including North America, Central America, western Europe, eastern Asia, and northern Africa. It remains unclear to what extent such megadrought require external forcing or whether they can arise from internal climate variability alone. A novel statistical-dynamical approach is used to evaluate the possibility that such events arise solely as a function of interannual tropical sea surface temperature (SST) variations. A statistical emulator of tropical SST variations is constructed by using an empirical moving-blocks bootstrap approach that randomly samples multi-year sequences of the observational SST record. This approach preserves the power spectrum, seasonal cycle, and spatial pattern of El Niño-Southern Oscillation (ENSO) but removes longer timescale fluctuations embedded in the observational record. These resampled SST anomalies are then used to force an atmospheric model (the Community Atmosphere Model Version 5). As megadroughts emerge in this run, they should, therefore, be solely a consequence of La Niña sequences combined with internal atmospheric variability and persistence driven by soil moisture storage and other land surface processes. We indeed find that megadroughts in this simulation have an amplitude-duration rate that is generally indistinguishable from the rate documented in paleoclimate records of the western United States. Our findings support the idea that megadroughts may occur randomly when the unforced climate system evolves freely over a sufficiently long period of time, implying that an unforced unusual but statistically plausible series of la Niña events may be sufficient to generate megadrought.

1. Introduction

Megadroughts are multidecadal periods of aridity as severe as the 1930s "Dust Bowl", but much longer lasting (Woodhouse and Overpeck, 1998; Ault et al., 2014; Cook et al., 2016; Ault and George, 2018). During the past millennium, paleoclimate records indicate that megadroughts occurred throughout the western US, northern Mexico, and many other parts of the world (Cook et al., 2016). Their long duration may have imposed unprecedented water stresses on several pre-industrial civilizations, contributing to their collapse (e.g., Benson et al., 2007; Cook et al., 2016). Furthermore, the odds that they will occur during this millennium are increasing due to rising regional temperatures and global circulation patterns (Ault et al., 2014; Cook et al., 2015; Ault et al., 2016). Despite the importance of characterizing the hazards imposed on water resources by megadroughts, it remains unclear whether such prolonged climate events in the past emerge in response to exogenous radiative forcing (e.g., solar irradiance, volcanic eruptions, or orbital trends), as a consequence of internal climate variability on multidecadal to centennial timescales (e.g., Coats et al., 2013; Stevenson et al., 2015; Ault et al., 2018), or as a function of unusual, but unforced, drought episodes on interannual timescales that collectively produce a megadrought (Coats et al., 2015; Ault et al., 2018). Here we explore this possibility by asking if an unusual, but inherently random series of La Niña events would be able to produce megadroughts.

Because megadroughts are infrequent events that have only occurred once or twice per millennium, two basic approaches have been employed to understand their nature using both dynamical or statistical models (e.g., Coats et al., 2015; Stevenson et al., 2006; Cook et al., 2016; Ault et al., 2018; Steiger et al., 2019). The first approach uses general circulation models (GCMs) of varying degrees of complexity to simulate fluctuations in the ocean and atmosphere that may lead to megadrought in millennial-scale simulations (e.g., Hunt, 2006; Coats et al., 2015; Stevenson et al., 2015; Stevenson et al., 2018). The advantage of this approach is that it links prolonged droughts to their physical and dynamical causes in the climate system. However, there are a few critical drawbacks for evaluating the possibility that an unusual sequence of La Niña events could cause megadroughts. First, GCMs do not always reproduce observed teleconnections between the tropical Pacific and the western US (Coats et al.,2013a), nor do their teleconnection strengths remain stable on multi-century timescales (Coats et al.,2013b). Second, GCMs often simulate ENSO variations that are too frequent and too energetic on interannual timescales (e.g., Guilyardi et al., 2009; Ault et al., 2013a); this exceptionally energetic ENSO variability, in turn, makes it extremely unlikely that any given simulation will see an “unusual” sequence of La Niña events because the tropical Pacific frequently switches states between La Niña and El Niño conditions. Finally, the simulations to-date using GCMs to characterize megadroughts either use a fully-couple global ocean, which makes it impossible to isolate the effects of the tropical Pacific on megadrought statistics, or an atmosphere-only model with climatological SSTs (e.g., Stevenson et al., 2015), which does not include El Niño and La Niña variations.

As an alternative to the GCM-based approach to characterizing megadrought, several studies have developed statistical models of drought using sea surface temperature (SST) anomalies based on empirical relationships (e.g., Coats et al., 2013; 2015; Ault et al., 2018). For example, using a linear inverse model (LIM) of internal climate variability, Ault et al. (2018) found that the frequency, magnitude, and spatial scale of megadroughts during the last millennium are consistent with the statistics of an unforced climate system. While Ault et al. (2018) established a "robust" null hypothesis for the occurrence of megadrought in the western US, the study was not designed to simulate the dynamic circulation patterns in the atmosphere. Moreover, the authors employed a LIM with nearly global sea surface temperature (SST) anomalies, meaning that the statistical relationships responsible for pushing the western US into megadrought could originate from high-latitude sources of low frequency variability (e.g., the Atlantic Multi-decadal Oscillation or the Pacific Decadal Oscillation).

From the noted four characteristics—frequency, magnitude, spatial scale, and mean-shift—that could define megadroughts (Ault et al., 2018), the mean-shift of the climate during the Medieval Climate Anomaly (MCA) era is a key component for the predominant clustering of megadrought (Coats et al., 2016), where intensification of droughts is not possible if the shifting is artificially removed. Attempts to identify the source of this clustering remain inconclusive (Coats et al., 2016; Ault et al., 2018). Thus, the MCA climate shift is critical because the clustering of the megadrought events. This finding opens the question whether its source is due to low-frequency variability in the Pacific or Atlantic. Although results on this matter are still inconclusive, new global climate reconstructions (e.g., the Paleo Hydrodynamics Data Assimilation, PHYDA, Steiger et al., 2019; 2021) or synthetic climate simulation, as we propose here, can give clues for further exploration of the low-frequency climate variability role in the MCA climate shift.

Here we test whether or not the tropical Pacific alone could generate megadroughts by using a bootstrap methodology to construct a synthetic SST forcing field with realistic sequences of El Niño and La Niña events. Therefore, we evaluate how well the method satisfies a series of criteria that warrant a realistic pattern of SST, in which ENSO evolution and its randomness play an important role. Such a methodology would therefore allow us to ask whether an inherently random series of interannual variations, along with internal atmospheric variability, could produce megadroughts in the SWUS.

2. Methods and datasets

2.1. Experimental design

a. Constructed synthetic sea surface temperature

The key component of our experimental design is the construction of the SST. Here we constructed a 1000-year long synthetic SST datasets. Our synthetic SST should preserve four characteristics of the historical record: (1) the ENSO signature in the power spectrum at the interannual scale; (2) the spatial patterns of SST anomalies to ensure that the forcing driving of the atmospheric component in the model is realistic; (3) the seasonal cycle of SST anomalies, so ENSO peaks in boreal winter; and (4) the evolution of the ENSO cycle with transitions from El Niño to La Niña embedded in the SST forcing fields. Therefore, the millennial synthetic SST field should isolate interannual variability in a long simulation to answer whether megadroughts can be generated as part of the natural variability without requiring an external forcing such as solar irradiance, volcanic eruptions, orbital trends, or high latitude SST variability. This allows us to answer whether the bootstrap method produces realistic teleconnections between the tropical Pacific and terrestrial hydroclimate when coupled to a GCM.

b. Moving-blocks bootstrap approach for constructing SST

The approach for generating the synthetic SST uses a moving-blocks (mv-Ba) bootstrap approach (Wilks 1997). In general, a bootstrap data generation emulates the statistics of a system by resampling a collection of a short original dataset (Wilks, 2011). In the moving-blocks bootstrap approach, randomization is done in blocks to preserve the seasonal evolution of ENSO but destroys any autocorrelation on low-frequency time scales. The resampling is done over a variable length segment of the original data that is defined by the duration of El Niño Southern Oscillation (ENSO) (**Fig. 1**), with the specific goal of retaining ENSO-like variability. Two constraints were used to guarantee conservation of seasonality and smooth continuity within the final time series. First, the default length of the mv-Ba bootstrap is 12 months for neutral years and variable for ENSO years (random between 2-7). Second, whenever the selected year is in El Niño or La Niña phase, we extend its original length with random values, so it always starts in January and ends in December. The bootstrap sampling process is done with the Niño 3.4 index (Trenberth, 1997) as reference, so we have the original sequence of El Niño and La Niña events with the block construction over the total SST field. To generate the synthetic SST, monthly observational data from the period 1960-2007 is used as a sampling pool, and it is resampled with reordering. As a result, we get a different sequence of El Niño and La Niña events that is completely analogous to what occurred in the historical period. Historical SST data for this resampling originates from the NOAA extended reconstructed SST (ERSST; Smith et al, 2008).

c. The linear inverse model of SST

As in Ault et al. (2018), we used a LIM approach as a benchmark to compare against the result with mv-Ba, but the alternative millennial SST from LIM is not part of the CAM5 experiment (see next). The LIM generates "multivariate red noise", which is analogous to a first order autoregressive (AR(1)) process; commonly used to test the null hypothesis for a unidimensional time series such as $\frac{dX}{dt} = LX + \zeta$. In LIM, autocorrelation coefficients are constructed with a linear deterministic feedback metric (L), and we use a multidimensional field (X) instead of a unidimensional time series. In this framework, we define X with three fields: sea surface temperature, sea surface height, and Palmer drought severity index (PDSI; Palmer 1965). ζ is the stochastic white noise forcing, which generates the variance that perturbs the linear system. For further details see Ault et al. (2018).

2.2. The Community Atmosphere Model

The SST generated with the mv-Ba procedure is used to force the Community Atmospheric Model version 5 (CAM5). To the extent possible, our simulations follow a similar experimental design to the control runs in the Last Millennium Ensemble (LME; Otto-Bliesner et al., 2016). Our simulations use CAM5 with prescribed SST in the tropics between 20°S and 20°N as in the Tropical Ocean - Global Atmosphere (TOGA) coupled ocean atmosphere experiments (Webster and Lukas, 1992; Gates, 1992; Phillips, 1996; Hurrell et al., 2008; Deser et al., 2017). We also use fixed ice configuration (Rayner et al., 2006), with 1980-2007 climatological ice concentration. Both SST and ice are interpolated in time to center the data at the middle of each month (Taylor et al., 2000). Total solar irradiance (TSI) and orbital parameters are fixed to the year 850 AD for the entire run. CAM5 is used under the modeling framework of the Community Earth System Model (CESM; Hurell et al., 2013) version 1.2.2 with 30 vertical levels in the atmosphere (from the surface to 2 mb) and 15 soil levels (from the surface to 35 meters ground). The horizontal resolution for this experiment is 1.9 x 2.5 degrees with finite volume (Lin and Rood, 1997).

2.3. Additional restrictions on SST

a. The tropical-extratropical transition zones

The synthetic SSTs are defined only in the tropical domain for both the mv-Ba SST and LIM SST between 20°S to 20°N (**Fig. S1**). Next, the tropical SST is merged with a climatological SST (annual cycle) from +/- 35° to the poles using the same data originally used to obtain the SST. Finally, the regions between 20°N-35°N and 20°S-35°S are linearly interpolated to reduce abrupt transitions from the tropics to the extratropics. This restriction is important because internal variability might play an important role in megadrought development during decadal and centennial scales (Coats et al., 2015).

b. Low-frequency signal in the SST

As in Ault et al. (2018), we removed the observed linear trend in SST over the length of the observations. Although the trend is small in the tropics, the mv-Ba model exhibited low-frequency SST variability due to the long sampling of the observed historical trend in sea surface temperature after 1960 (Mann et al., 2009). Using a linear regression method that does not change the statistics of the SST with the mv-Ba approach, the problem has been solved by removing the observational SST trend prior the calculation of the synthetic SST. Thus, the approach removes the global net radiative force-like term (Mann et al., 2009) obtained from a global average surface temperature (HadCRUT4, Osborn and Jones, 2014). We then use linear regression of this global surface temperature to fit SST data at each grid point. To avoid removing SST variability in the interannual time scale, the global surface temperature was smoothed using a 10-year running mean filter before the linear regression. Thus, the generated historical trend contain the observed global warming trend.

2.4. Statistical characteristics of megadrought

While the mv-Ba statistical model can be run hundreds of times for thousands of years, CAM5 cannot (at least, not with existing technology and a standard University Small Allocation on the Cheyenne supercomputer). We therefore run large numbers of realizations of the mv-Ba model, then examine the distributions of key statistics that describe the power spectrum, seasonality, and spatial patterns of tropical Pacific SST variability in these oceans. To identify megadroughts in our mv-Ba realizations, we use the same metrics as Ault et al., 2018, to characterize megadroughts by their duration, magnitude, and spatial scale. Specifically, we compute the 35-year running mean of PDSI ($PDSI_{35}$) from both reconstructions and model data, then use its minimum values over a 1000-year period to identify the "worst" prolonged event. To characterize the spatial scale of megadroughts in the western US, we calculate the fraction of the domain with $PDSI_{35}$ values below -1 standard deviation. This fraction is then used as a drought area index (DAI). Probability density functions (PDFs) are computed using each of these test statistics from the mv-Ba statistical model and compared against observations and new simulations.

2.5. The Last Millennium Ensemble experiment

We use the rich archive of model outputs from the Last Millennium Ensemble experiment (Otto-Bliesner et al., 2016), which are a set of simulations all based on the CESM with CAM5 as an atmospheric model. The LME experiment has the primary goal of exploring sources of uncertainty in the reconstruction of the external forcing that drives the climate of the past millennium. Here, the purpose is to check the skill of CAM5 (with LME and the in-house millennial simulation) to capture drought variability in the SWUS. We investigate whether the pattern in CAM5 simulation with mv-Ba is comparable with LME. We used the multiple simulations, a total of 35 for this study, to generate an approximation of the most probable scenario with several forcing simulations: volcanic eruption, changes solar irradiance, orbital, greenhouse gas level, land use-land cover, and the full forcing. That includes ensemble members with random perturbations of the order of 10^{-14}°C in the air temperature field at the initialization of the simulation. However, we do not make a distinction among the external forcings in the analysis at this point. We employed the first 1000 years from each simulation (850-1849) to avoid the post-industrial global warming era.

3. Results

3.1. Statistical characteristics of mv-Ba tropical SSTs

Do the mv-Ba statistical SST emulators preserve the power spectrum of ENSO on interannual timescales? The distribution of NINO3.4 power spectra generated by the mv-Ba statistical model is consistent with the characteristics of interannual variability in the tropics (**Fig. 2**) and similar to the LIM. Using 100 realizations (a total of 100,000 years) from both methods, both approaches can reproduce the observed spectral peaks at the interannual range (x-axis < 10 years) at the 95% confidence level. Specifically, the spectral density of the mv-Ba approach fully encompasses the range of spectral densities recorded in observational datasets across two-year to seven-year frequencies (gray shading, Fig. 2). On interdecadal timescale (x-axis > 10 years), spectral amplitude of both distributions decreases. Consequently, these attributes of the mv-Ba ensure that high amplitude, low-frequency (decadal- to century-scale) variability is not present in the SST forcing fields we later couple to CAM5.

Do our statistical SST fields exhibit realistic spatial patterns of tropical Pacific anomalies? The annual spatial pattern of variance in SST generated by mv-Ba is close to the one seen in observations (**Fig. S2**). The major variability occurs in the eastern Pacific Ocean. With this result, we can claim that at the annual scale the approach is indistinguishable from observations, which will explain later the convergence of the drought results at the long-term run in the CAM5 simulation. However, analyzing the variance at monthly scale, greater similarity exists within the mv-Ba results. The seasonal amplitude of variance in the NINO3.4 region in the mv-Ba distribution matches observations nearly identically (**Fig. 3**).

Do our statistical methods reproduce the seasonal cycle of SST variance and ENSO evolution? The mv-Ba approach resolves seasonality well, which does not require El Niño (and La Niña) events to be phase-locked to the annual cycle. As a result, applying mv-Ba to SST allows a realistic seasonal evolution of ENSO in the tropics (**Fig. 4**). Using moving blocks, we see transitions from El Niño to La Niña phase that peak in January of the El Niño year that are very similar to transitions seen in observed ENSO years. As in the observations (and in the mv-Ba approach), La Niña events tend to follow El Niño events. Nevertheless, the mv-Ba (by construction) does overall well at reproducing the observed seasonality of SSTs in the tropical Pacific, the phase locking of El Niño and La Niña events with the annual cycle, and the seasonal evolution of individual events.

Does the mv-Ba method reproduce realistic *statistics* of teleconnections between the tropical Pacific and terrestrial hydroclimate when coupled to CAM5? A correlation analysis between mv-Ba tropical SST (for El Niño 3.4 region) and statistically generated PDSI shows the typical out-of-phase PDSI pattern between the SWUS hydroclimate and the Pacific Northwest variability (**Fig. S3**). A positive relationship between PDSI, within the SWUS, and El Niño 3.4 index is evident in different realizations of the statistical climate. Several CESM simulations have shown a significant correlation between SST and PDSI. These findings are consistent with SST and PDSI from instrumental records (**Fig. 5**). Surprisingly, the variability of PDSI from CAM5-mv-Ba is consistent with observation, and it exhibits a more coherent pattern than the fully-coupled LME simulations. We suggest these matching patterns as evidence that key hydroclimate variability in SWUS is sourced from the tropical climate variability (Coats et at., 2013a). Since the LME is a fully coupled simulation, this difference to observations and the CESM-vs-Ba simulations might be due to the fixed SST forcing.

3.2. Megadroughts in a hybrid simulation

Equipped with a better understanding of the statistical behavior of the mv-Ba statistical SST generator, we now turn to our experiment where we couple one realization from the model to CAM5. In just one CAM5 run of 1000-year pre-sampled observations, there is an event as severe as the most severe event of the last millennial in the reconstructed Palmer Drought Severity Index for the SWUS (**Figs. 6 and 7**). Spatial patterns of drought metrics produced by CAM5-mv-Ba look as realistic as those in the observed paleoclimate records (Fig. 5). Both PDSI and Drought Area Index (DAI) identify megadrought in the simulated 1000-year record (Fig. 6). Composite analysis of these drought metrics for two different datasets, the mv-Ba SST and CAM5-mv-Ba SST, support our working hypothesis that megadroughts occur in both the stochastic (**Fig. S4**) and the dynamically-generated climate states (Fig. 7). This analysis suggests that tropical SST variability can drive megadrought based on random processes via the correct large-scale teleconnection. A composite analysis of SST_{35} (a 35-year running mean filter of SST) during megadroughts in SWUS shows a predominant La Niña-like pattern (Figs. 7 and S3; bottom), as La Niña has been linked to dry conditions in the SWUS (Seager et al., 2005; Herweijer et al., 2007), which is also observed in the LME experiment but with a minor impact over land (**Fig. 8**) and a weak ocean teleconnection (**Fig. 9**). Results from our previous work using LIM (i.e., Ault et al., 2018) are also consistent with this analysis, and they suggest a similar mechanism.

3.3. Megadrought statistics

The hybrid modeling approach (CAM5-mv-Ba) confirms the statistically significant occurrence of megadrought in the SWUS similar to paleoclimate records and LIM (**Fig. 10**). Results from CAM5-mv-Ba are compared with the probability density function of several LIM runs used as benchmark (cyan histogram in Fig. 10). As in Ault et al. (2018), we computed megadrought characteristics for the SWUS: (1) magnitude and (2) spatial scale. The null hypotheses for (1) and (2) were rejected at the 95% confidence level (Fig. 10), meaning that both the magnitude and spatial scale of megadroughts are also statistically significant in this experiment. Therefore, megadroughts as defined by their magnitude and spatial scale may occur as a result of internal climate variability and random La Niña-like SST pattern.

a. The magnitude of megadrought: $PDSI_{35}$

The drought magnitude statistic is defined by the probability density function in the cyan histogram (Fig. 10a) with mean $PDSI_{35}$=-0.6. This cyan histogram represents the minimum $PDSI_{35}$ value over a 1000-year time series with a total pool of 1000 samples. The primary sample pool was obtained from the 1000-year CAM5-mv-Ba control run. The secondary sample pool was generated by resampling a 100-year time series of both the PDSI and SST from this CAM5-mv-Ba run, then using a LIM to stochastically generate a new 1000-year stochastic $PDSI_{35}$ (Ault et al., 2018). The marks (*, x, and + in Fig. 10a) are computed in the same way but using PDSI from the North American Drought Atlas (NADA; Cook et al., 2010) and PDSI from the CAM5-mv-Ba bootstrap. The NADA is the driest event. PDSI was computed from CAM5-mv-Ba after the atmospheric model runs forced by the SST were allowed to generate the moisture anomalies in the SWUS. This analysis shows that megadrought magnitude observed in tree-ring chronology is part of the LIM-PDSI distribution based on CAM5-mv-Ba at the 95% confidence level (indicated by the light gray region). In addition, Fig. 6 shows that it is statistically significant. The parameter distribution shows that the NADA megadrought intensity during the MCA is not an extreme case, but one that is in 90% (probability of PDSI35 be more intense than the case measured in NADA, $Pr\,\{X \leq x(NADA)\} = 0.9$ from Fig. 10a) of the “classical” megadrought. Therefore, megadrought of higher intensity than the one found in the paleoclimate tree-ring record are possible and thus can be expected in the future.

b. The spatial scale of megadrought: DAI_{35}

The spatial scale of megadrought in the SWUS also shows statistically significant results (Fig. 10b). For this we use a slightly different approach from Ault et al. (2018), but with similar conclusions. Here we introduce the scaled drought area index, scaled-DAI_{35} = $PDSI_{35} \cdot DAI_{35}$, because it is conservative for different PDSI thresholds. As DAI_{35} and $PDSI_{35}$ for the SWUS have an inverse linear relationship for extreme values (**Fig. S5**), analyzing DAI_{35} using different area thresholds makes analysis not generalized. However, scaling DAI (by multiplying it by its PDSI value) eliminates values that are not relevant for megadrought statistics, for example, values close to zero for both PDSI and DAI. Therefore, the scaled-DAI_{35} provides a generalized parameter that is conservative along different PDSI thresholds that are used to compute DAI. As noted in the supplementary material, the peak of the scaled-DAI_{35} distribution is near the same value (e.g., -15 scaled-DAI_{35} units) for different PDSI thresholds (**Fig. S6**). Therefore, scaled-DAI_{35} is conservative against changes of PDSI. Using this new scaled-DAI_{35} distribution (Fig. 12b), we show that megadrought spatial scale as computed with tree-ring chronologies (NADA), mv-Ba, and CAM5-mv-Ba are part of the same statistically-dynamically generated pool of megadrought distribution (cyan histogram).

4. Conclusions

Our experiments show that SWUS megadroughts are not conditionally linked to low-frequency variability in the tropical Pacific. A synthetic tropical SST is constructed to test the significance of megadrought occurrence driven by a series of La Niña events. This synthetic SST is stochastically sampled from the current climate (1960-present) but detrended to reduce observed warming trend signals. We sampled observations focusing on interannual rather than decadal or centennial SST variability. Still, our approach preserves the power spectrum, seasonal cycle, spatial pattern, and ENSO evolution. The so constructed synthetic climate reproduces megadrought statistics similar to those achieved in the stochastic linear inverse model of Ault et al. (2018). With respect to a robust null hypothesis test, this study claims that the spatial scale and magnitude of megadrought in the SWUS are generated from natural variability of the interannual climate regime. This provides additional evidence that decadal variability could arise from internal variability at the interannual scale (Newman et al., 2016). In addition, our experiment isolated any potential low-frequency variability memory of the Atlantic Ocean, which raises questions about previous findings that relate Atlantic Ocean variability to SWUS megadrought (Seager et al., 2008). For paleoclimate research, our approach can help to test the significance of the low-frequency signal in the tree-ring chronologies, as this approach merges current statistical knowledge of the climate with an extension of potential synthetic climate scenarios.

The CAM5 hybrid setting seems to properly simulate a megadrought type of climate in the SWUS, even at a relatively coarse spatial resolution. Certainly, this simulation is possible with the idealized ocean that is statistically indistinct from observations. As speculated in Coats et al. (2013), both stochastic atmospheric variability and ENSO are capable of producing megadrought in the SWUS. However, further investigation is required to determine whether internal atmospheric variability alone can generate 35-year droughts, and not just shorter 15-year megadrought (Stevenson et al., 2015). For climate change projections, the presented results motivate further exploration of this hybrid modeling framework to evaluate the impact of external forcing: solar irradiance, volcanic eruptions, and orbital trends. The CAM5-PDSI analysis validates the previous finding of megadrought characteristics using the stochastic LIM approach (Ault et al., 2018). Composite and spectral analyses of SST and PDSI shows strong teleconnection patterns among observation and CAM5-mv-Ba, something not seen in a fully-coupled LM simulation (Mann et al., 2009; Landrum et al., 2013), which supports the legitimacy of this experiment. Our previous work (Ault et al., 2018) shows that the worst event described in the NADA is not significantly different from the LIM-based null hypothesis. The worst event in the mv-Ba bootstrap experiment is also consistent with the null hypothesis. The mv-Ba SST designed here reproduces megadrought, as noted by its spectral-temporal and spatial patterns, and therefore it makes this approach a reasonable candidate for building other statistics to test in the SWUS megadrought.

Nevertheless, the tests over two of the megadrought statistics (clustering and shift of mean) were not rejected. This expected result motivates the implementation of additional experiments. We will use the CAM5 to conduct new experiments to characterize the role of dust, ocean surface temperatures, solar forcing, and land-surface feedbacks in making megadroughts more clustered. We are planning these simulations with these LIM and mv-Ba bootstrap approaches that use an idealized forcing to test whether or not we get a drier mean climate. Such simulations will include solar, dust variability, and prognostic vegetation, which may potentially be relevant for driving a mean climate shift during the medieval climate anomaly (MCA). In particular, megadroughts in the southwest appear to have "clustered" around the MCA. State-of-the art model simulations do not reproduce that clustering, nor do they simulate the MCA as being drier on average than more recent centuries (e.g., Coats et al., 2016). Our results here provide new insights into the possibility that megadrought conditions will be seen this century, and they will ultimately help scientists and stakeholders alike to prepare for such events if they do unfold in the western United States.

Acknowledgment

The authors thank NCAR for the use of its computing facilities. The simulations were performed at the NCAR-Wyoming supercomputer. The CESM project is supported primarily by the National Science Foundation (NSF). This work was partially supported by the P2C2 NSF Grant No. 1602564.

Open research

The CESM model were provided by NCAR-UCAR. The Last Millennium Ensemble (LME) dataset is from the CESM Paleoclimate Working Group at NCAR and available via the Climate Data Gateway at NNCAR: http://www.earthsystemgrid.org .

References

Ault T.R., George St. S., 2018. Unraveling the mysteries of megadrought. Physics Today 71(8):44-50.

Ault T.R., George S. St., Smerdon J.E., Coats S., Mankin J.S., Carrillo C.M., Cook B.I., Steveson S., 2018. A robust null hypothesis for the potential causes of megadrought in western north America. Journal of Climate 31: 3-24.

Ault T.R., Cole J.E., Overpeck J. T., Pederson G. T., Meko D. M., 2014. Assessing the risk of persistent drought using climate model simulations and paleoclimate data. Journal of Climate 27: 7529– 7549, doi:10.1175/JCLI-D-12-00282.1.

Ault T.R., Mankin J., Cook B. I., Smerdon J. E., 2016. Relative impacts of mitigation, temperature, and precipitation on 21st-century megadrought risk in the American Southwest. Sci. Adv., 2, e1600873, doi:10.1126/sciadv.1600873.

Benson L, Petersen K, Stein K (2007) Anasazi (Pre-Columbian Native-American) migrations during the middle-12th and late-13th centuries—Were they drought induced? J Clim Change 83:187–213. doi: 10.1007/s10584-006-9065-y

Carrillo C.M., Castro C.L., Garfin G., Chag H.I., Bukovsky S.M., Mearns L.O., 2018. Pacific sea surface temperature related influences on North American monsoon precipitation within North American Regional Climate Change Assessment Program models. International Journal of Climatology 38: 4189-4210.

Coats S., Smerdom J.E., Seager R., Cook B.I., Gonzáles-Rouco J.F., 2013. Megadroughts is Southwestern North America in ECHO-C Millennial Simulations and their comparison to proxy drought reconstruction. Journal of Climate 26: 7635-7649.

Coats S., Smerdon J. E., Cook B. I., Seager R., 2015. Are simulated megadroughts in the North American Southwest forced? J. Climate, 28, 124–142, doi:10.1175/JCLI-D-14-00071.1.

Cook B.I., Ault T. R., Smerdon J. E., 2015. Unprecedented 21st century drought risk in the American Southwest and central plains. Sci. Adv., 1, e1400082, doi:10.1126/sciadv.1400082.

Cook E.R., Seager R., Heim Jr R.R., Vose R.S., Herweijer C., Woodhouse C., 2010. Megadroughts in North America: placing IPCC projections of hydroclimatic change in a long-term palaeoclimate context. Journal of Quaternary Science, 25, 48-61.

Davis K.F., Bhattachan A., D'Odorico P., Suweis S., 2018. A universal model for prediction human migration under climate change: examining future sea level rise in Bangladesh. Environmental Research Letter 13. https://doi.org/10.1088/1748-9326/aac4d4

Gates W. L., Boyle J., Covey C., Dease C., Doutriaux C., Drach R., Fiorino M., Gleckler P., Hnilo J., Marlais S., Phillips T., Potter G., Santer B., Sperber K., Taylor K., Williams D., 1998. An Overview of the Results of the Atmospheric Model Intercomparison Project (AMIP I). *Bulletin of the American Meteorological Society*, 73, 1962-1970.

Guilyardi E., Braconnot P., Jin F-F., Kim S.T., Kolasinski M., Li T., Musat I., 2009. Atmosphere Feedbacks during ENSO in a Coupled GCM with a Modified Atmospheric Convection Scheme. *Journal of Climate*, 22, 5698-5718.

Herweijer C., Seager R., Cook E.R., Emile-Geay J., 2007. North American droughts of the last millennium form a gridded network of tree-ring data. Journal of Climate 20: 1353-1376.
Howitt R., Medellin-Azuara J., MacEwan Duncan, Lund Jay, Sumner D., 2014. Economic analysis for the 2014 drought for California agriculture. Center for Watershed Scienecs. University of California, Davis, CA. 20p. http:/watershed.ucdavis.edu. Accessed Aug 27, 2017.

Hurell J., Holland M.M., Gent P.R., Ghan S., Kay J.E., Kushner P.J., Lamarque J.F., Large W.G., Lawrence D., Linsay K., Lipscomb W.H., Long M.C., Mahowald N., Marsh D.R., Neale R.B., Rasch P., Vavrus S., Vertenstein M., Bader D., Collins W.D., Hack J.J., Kiehl J, Marshal

S., 2013. The Community Earth System Model: A framework for collaborative research. Bulleting of the American Meteorological Society 94: 1339-360.

Landrum L., Otto-Bliesner B., Wahl E.R., Conley A., Lawrence P., Rosenbloom N., Teng H., 2013. Last Millenium climate and its variability in CCSM4. Journal of Climate 26: 1085-111.

Lin S.J., Rood R.B., 1997, An explicit flux-form semi-lagrangian transport shallow water model on the sphere, Q. J. R. Meteorological Soc. 123, 2531-2533.

Mann M.E, Zhang Z., Rutherford S, Bradley RS, Hughes M.K., Shindell D., Ammann C., Faluvegi G., Ni F., 2009. Global signatures and dynamical origins of Little Ice Age and Medieval Climate Anomalies. Science, 326, 1256-1260.

Meehl G.A., Hu A.X., 2006. Megadroughts in the Indian monsoon region and southwest North America and a mechanism for associated multidecadal Pacific sea surface temperature anomalies. Journal of Climate 19: 1605-1632.

Mlawer E., Taubman S., Brown P., Iacono M., Clough S., Radiative transfer for inhomogeneous atmospheres: Rrtm, a validated correlated-k model for the longwave, Journal of Geophysical Research 102:16663-16682.

Morrison H., Gettelman H., 2008. A new two-moment bulk stratiform cloud microphysics scheme in the NCAR Community Atmosphere Model (CAM3). Part I: Description and numerical tests. Journal of Climate 15: 3642-3659.

Newman M., Alexander M.A., Ault T.R., Cobb K.M., Deser C., Di Lorenzo E., Mantua N.J., Miller A.J., Minobe S., Nakamura H., Schneider N., Vimont D.J., Phillips A.S., Scott J.D., Smith C.A., 2016. The Pacific Decadal oscillation, revisited. Journal of Climate 29: 4399-4427.

Osborn T.J., Jones P.D., 2014. The CRUTEM4 land-surface air temperature data set: construction, previous versions and dissemination via Google Earth. *Earth System Science Data* 6, 61-68, doi:10.5194/essd-6-61-2014.

Otto-Bliesner B, Brady E.C., Fasullo J., Jahn A., Landrum L., Stevenson S., Rosenbloom N., Mai A., Strand G., 2016. Climate variability and change since 850 CE: An ensemble approach with the community Earth System Model. Bulletin of the American Meteorological Society 97:735-754.

Park S., Bretherton C.S., 2009. The University of Washington shallow convection and moist turbulence schemes and their impact on climate simulations with the community atmosphere model. Journal of Climate 22:3449-3469.

Penland C., 1989. Random forcing and forecasting using principal oscillation pattern analysis. Monthly Weather Review 117: 2165-2185.

Rayner N.A., Parker D.E., Horton E.B., Folland C.K., Alexander V., Rowell D.P., Kent E.C., Kaplan E.C., 2006. Global analyses of sea surface temperature, sea ice, and night marine air temperature since the late nineteenth century. Journal of Geophysical Research: Atmosphere 108: 1-29

Seager R., Kushnir Y., Herweijer C., Naik N., Velez J., 2005. Modeling of tropical forcing of persistent droughts and pluvials over western North America: 1856-2000. Journal of Climate 18: 4065-4088.

Seager R., Kushnir Y., Ting M., Cane M., Naik N., Miller J., 2008. Would advance knowledge of 1930s SSTs have allowed prediction of the Dust Bowl drought? Journal of Climate 21: 3261-3281.

Smith TM., Reynolds RW., Peterson TC., Lawrimore J., 2008. Improvements to NOAA's historical merged land-ocean surface temperature analysis (1880-2006). Journal of Climate 21: 2283-2296.

Steiger N.J., Smerdon J. E., Cook B. I., Seager R., Williams A. P., Cook E. R., 2019. Oceanic and radiative forcing of medieval megadroughts in the American Southwest. Science Advances 5(7): eaax0087

Steiger N. J., Smerdon J. E., Seager R., Williams A. P., Varuolo-Clarke A.M., 2021. ENSO-driven coupled megadroughts in North and South America over the last millennium. Nature Geoscience, 14: 739-744.

Stevenson S., Timmermann A., Chikamoto Y., Langford S., DiNezio P., 2015. Stochastically generated North American Megadroughts. Journal of Climate 28: 1865-1880.

Taylor K.E., Williamson D., Zwiers F., 2000. The sea surface temperature and sea-ice concentration boundary conditions for AMIP II simulations. PCMDI Report No 60, 24 pp.

Trenberth K.E., 1997. The definition of El Niño. Bulletin of the American Meteorological Society 78(12): 2771-2777.

United Nation High Commissioner for Refugees (UNHCR) agency. 2018. Venezuelan exodus to Ecuador reaches record levels: UN refugee agency steps up aid. United Nations News. https://news.un.org/en/story/2018/08/1016812. Accessed Sep 10, 2018.

Wilks D.S., 1997, Resampling hypothesis tests or autocorrelated fields. Journal of Climate 10:65-82.

Wilks D.S., 2011. Statistical methods in the atmospheric sciences. Academic Press. Elsevier. 676.

Woodhouse C.A., Overpeck J.T., 1998. 2000 years of drought variability in the central United Stated. Bulleting of the American Meteorological Society 79:2693-2714.

Zhang G.J., McFarlane N.A., 1995. Sensitive of climate simulations to the parameterization of cumulus in the Canadian Climate Centre general circulation, Atmosphere-Ocean 33: 407-446.

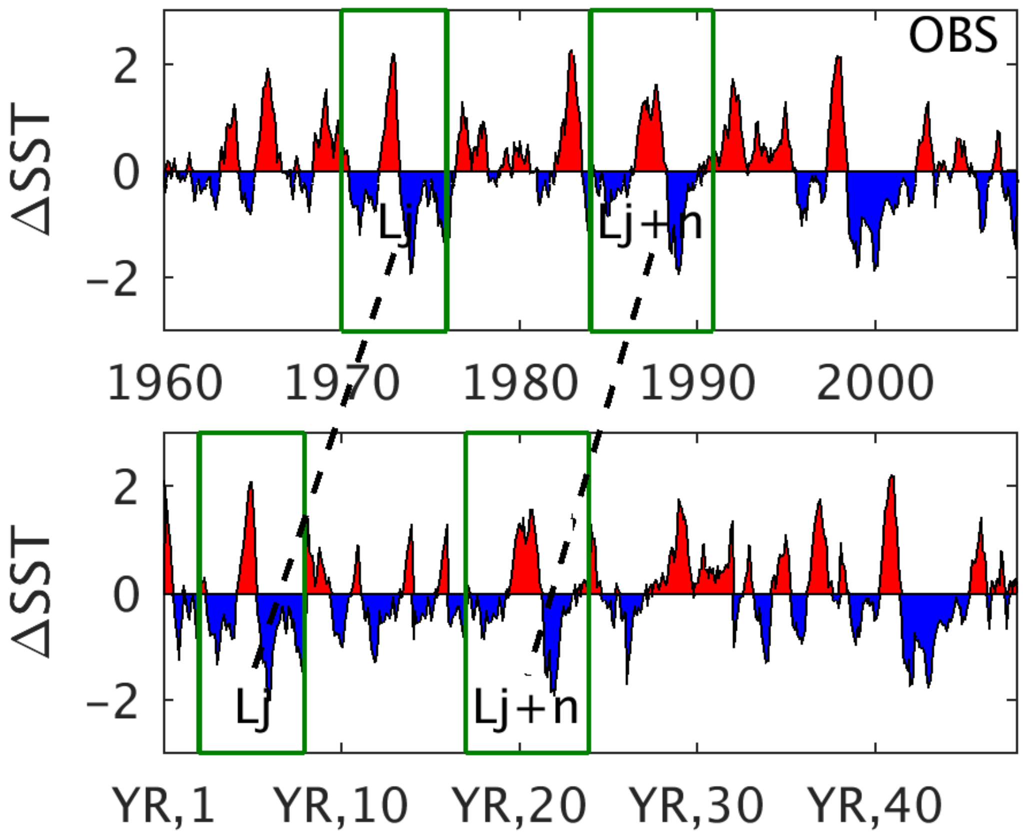

Figure 1: El Niño 3.4 region (NINO3.4) time series to illustrate the moving-blocks bootstrap (mv-Ba) methodology. The upper plot is the observational (OBS), original NINO3.4 sea surface temperature (SST) used as the database for constructing the synthetic moving-blocks bootstrap SST. An example one realization moving-blocks bootstrap approach is shown in the lower plot for 57 years and the x-axis labeled in blocks of 10 years (YR). The green boxes show the construction for two moving-blocks bootstrap of different lengths that are highlighted as an example and labeled as Lj and Lj+n.

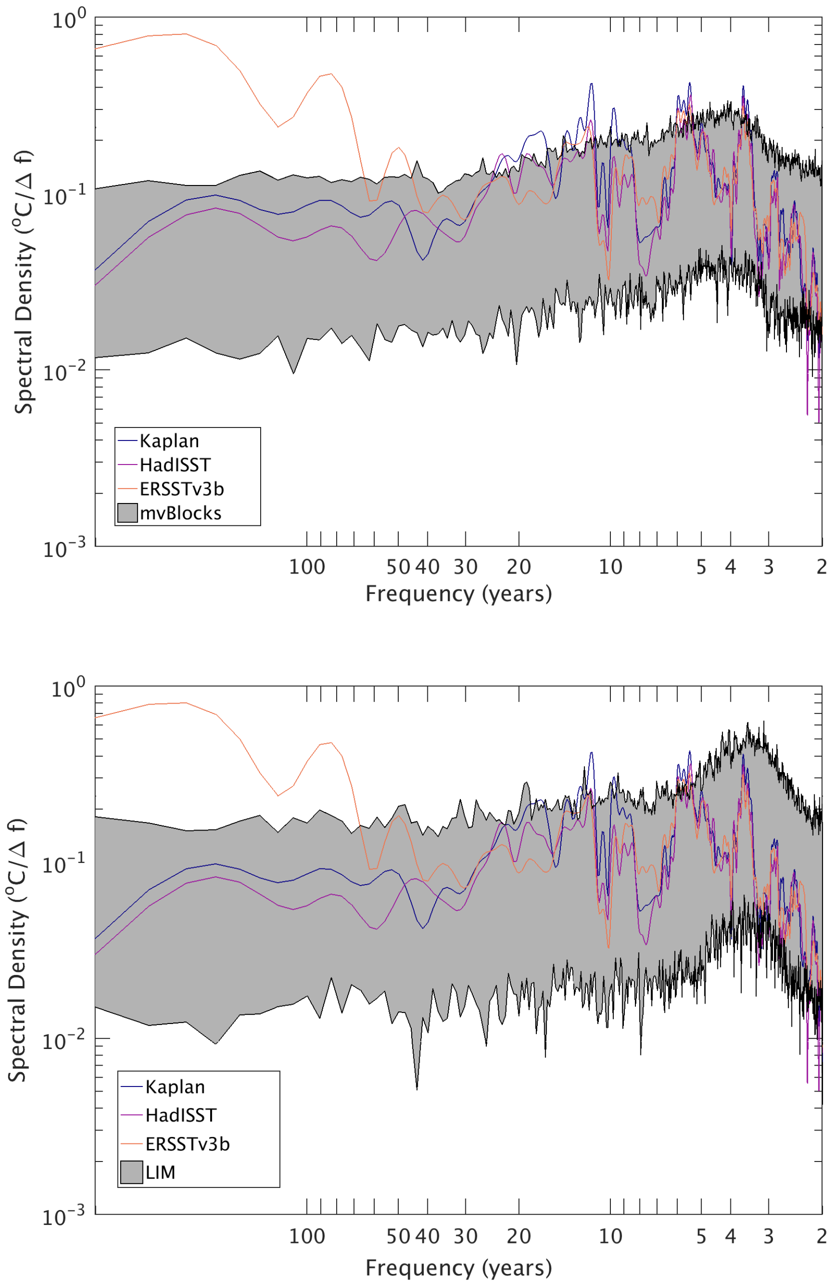

Figure 2: Top: Upper and low 95% confidence limits of NINO3.4 power spectra computed from 100 stochastically generated moving-blocks bootstrap realizations (confidence limits shown in gray shading), and three different observational SST data products: Kaplan, HadISST, and ERSSTv3b. Bottom: same analysis as top panel but for SST constructed with the Linear Inverse model (LIM).

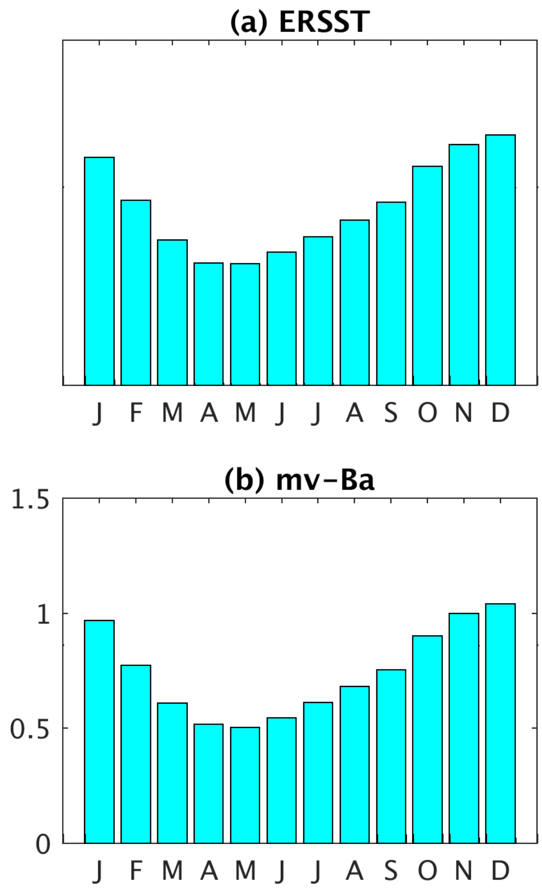

Figure 3: Monthly standard deviation for NINO3.4 region from observation (a) from the extended reconstructed sea surface temperature (ERSST) and (b) the moving-blocks bootstrap (mv-Ba) statistical approach employed here.

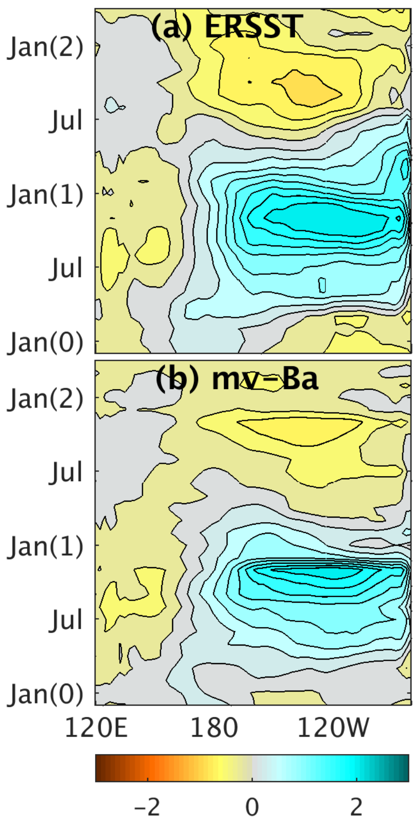

Figure 4: Hovmoller diagrams of seasonal evolution of tropical [5°S-5°N] sea surface temperature (SST) anomaly for two datasets: (a) the extended reconstructed SST (ERSST) and (b) the moving-blocks bootstrap (mv-Ba) SST. The diagrams are composite for El Niño events identified in these databases for its entire life cycle starting in January of the onset year, Jan(0), and ending two years after, Jan(2).

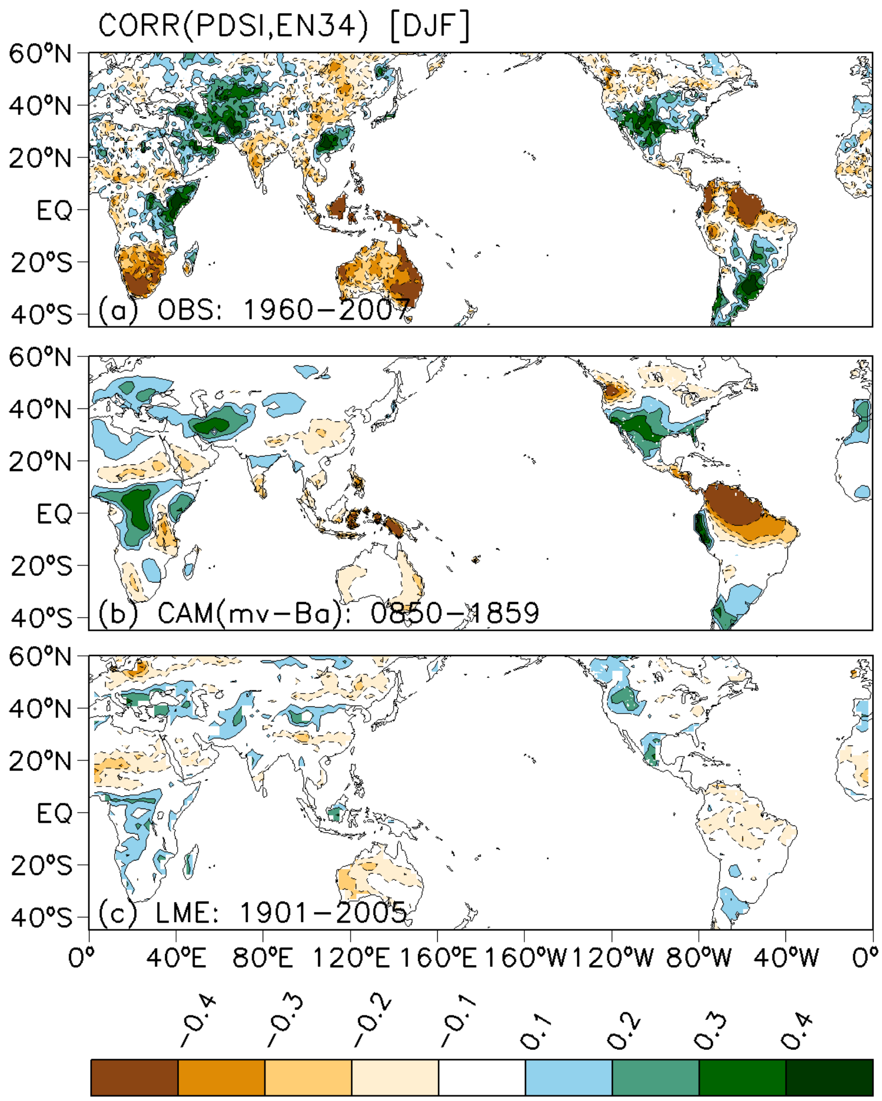

Figure 5: Correlation winter patterns (December-January-February, DJF) between El Niño 3.4 sea surface temperature (SST) index and Palmer Drought Severity Index (PDSI) for four databases: (a) observational data from the extended reconstructed SST and PDSI from Sheffield et al., 201X; (b) SST and PDSI obtained from a CAM simulation driven with SST randomly obtained from the moving-blocks bootstrap approach, CAM(mv-Ba); and (c) SST and PDSI obtained from a simulation from the Last Millennium Ensemble (LME).

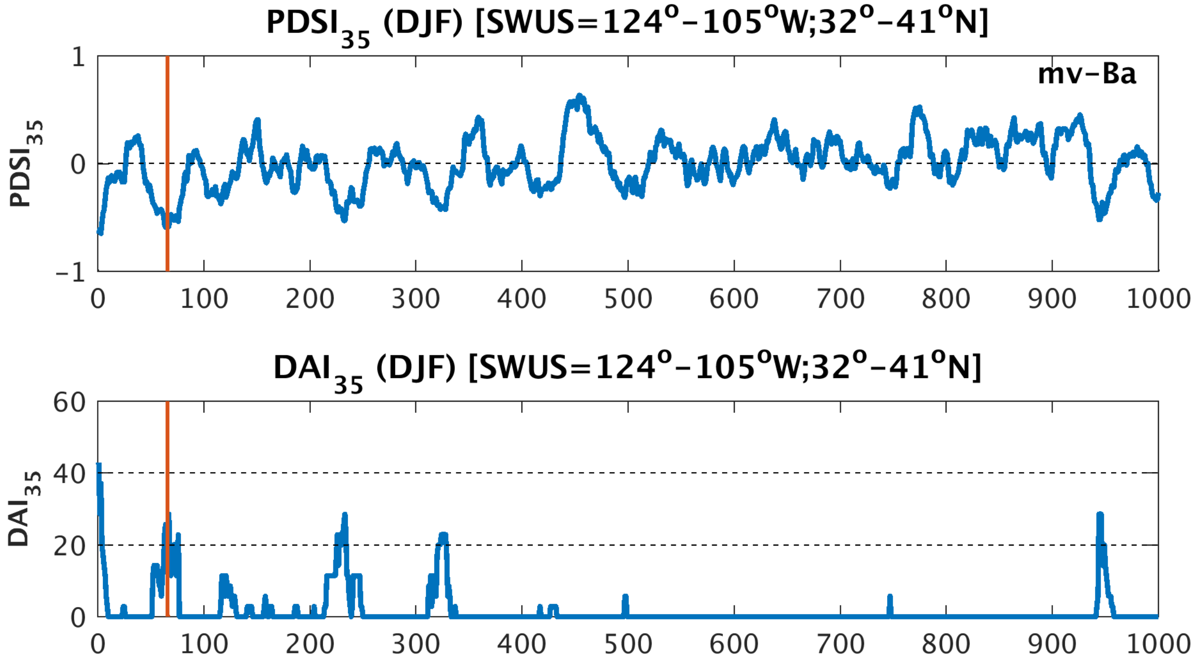

Figure 6: Palmer Drought Severity Index (PSDI) and Drought area index (DAI) time series defined over the SWUS region (124°-105°W and 32°-41°N) from the CAM5-mv-Ba simulation with sea surface temperature (SST) generated by the moving-block (mv-Ba) bootstrap approach, showing one candidate for megadrought events (DAI > 20%) as highlighted with the vertical solid line. The PDSI and DAI time series were smoothed with a 35-year running mean average filter, PDSI35 and DAI35.

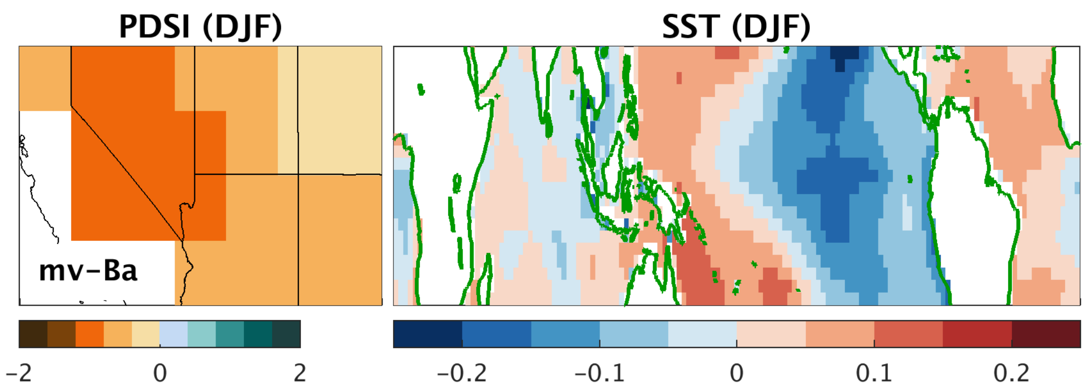

Figure 7: Palmer Drought Severity Index (PSDI) and sea surface temperature (SST) for a megadrought case using a CAM5 simulation for the moving-block (mv-Ba) approach. The case is the one identified in the Figure 6, so the panels are the average fields over 35-years that defined the megadrought duration indicated by the vertical line in the DAI35 time series.

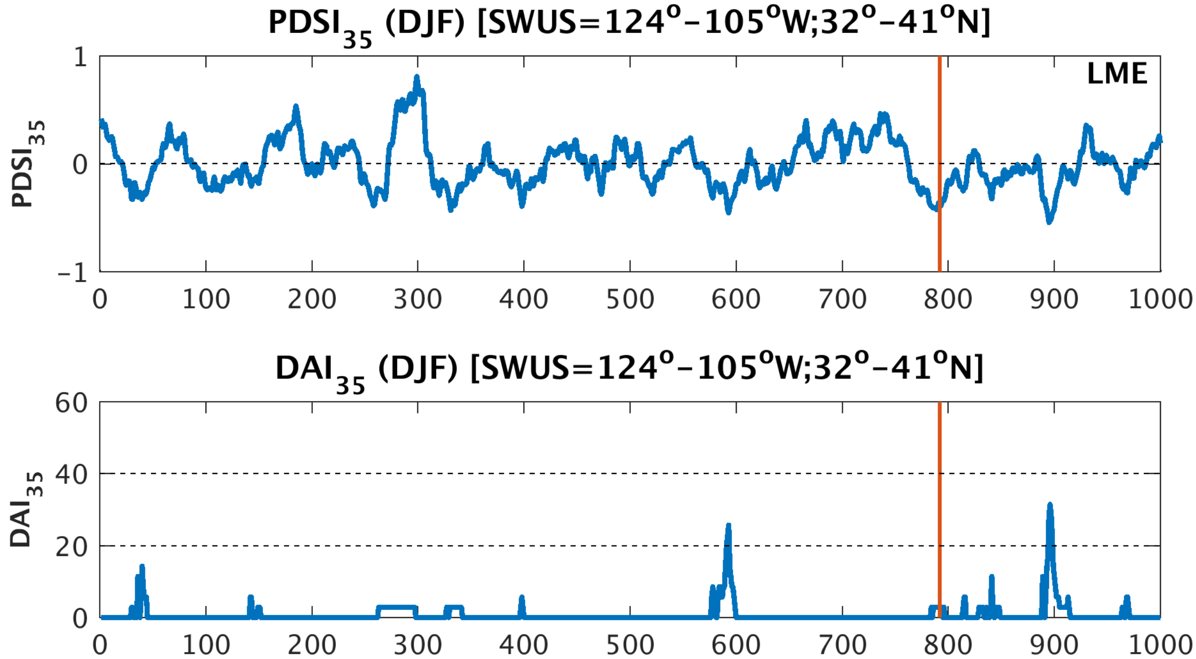

<u>Figure 8</u>: Palmer Drought Severity Index (PSDI) and Drought area index (DAI) time series defined over the SWUS region (124°-105°W and 32°-41°N) that shows one poor candidate for megadrought events (DAI < 20% but PDSI < -0.5) as highlighted with the vertical solid line. The PDSI and DAI time series were smoothed with a 35-year running mean average filter, PDSI35 and DAI35. These time series correspond to the first millennium of the Last Millennium Ensemble (LME) experiment.

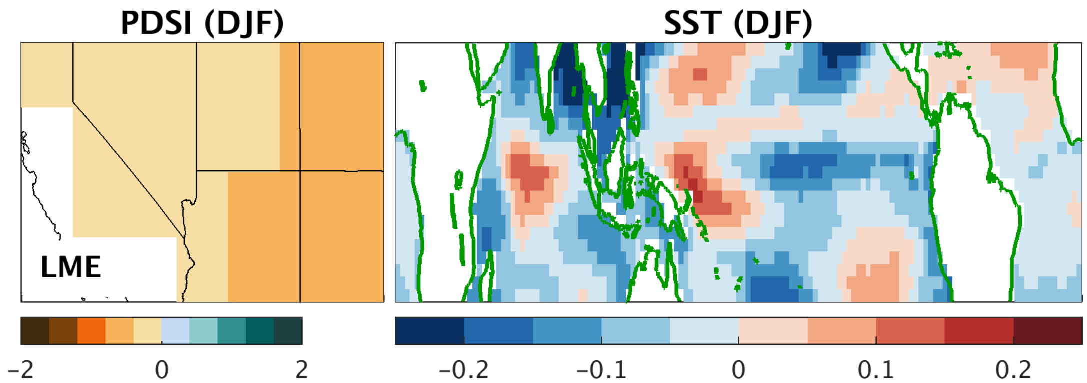

Figure 9: Palmer Drought Severity Index (PSDI) and sea surface temperature (SST) for a megadrought case using a simulation of the Last Millennium Ensemble (LME) experiment. The case is the one identified in the Figure 8, so the panels are the average fields over 35-years that defined the megadrought duration indicated by the vertical line in the DAI35 time series.

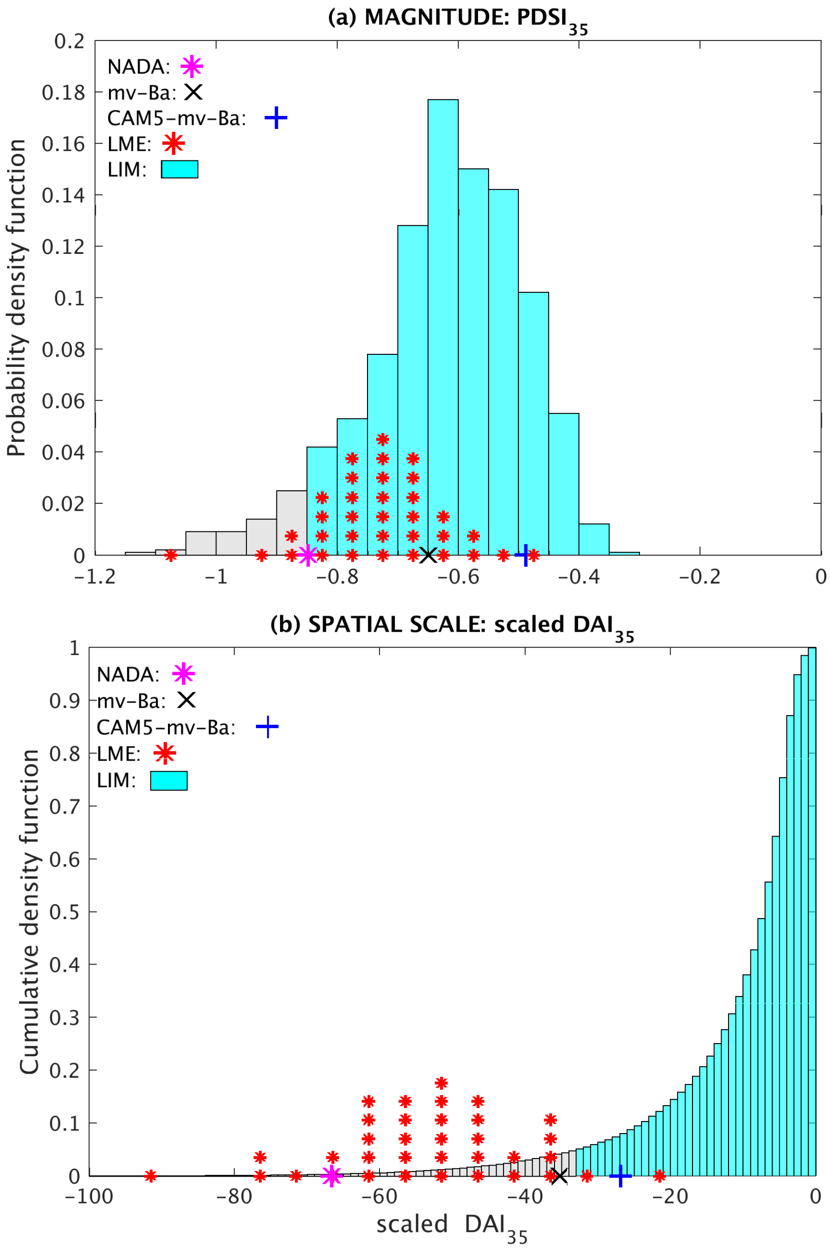
(a) MAGNITUDE: PDSI35
NADA:
mv−Ba:
CAM5−mv−Ba:
LME:
LIM:
Probability density function
0.2
0.18
0.16
0.14
0.12
0.1
0.08
0.06
0.04
0.02
0
−1.2
−1
−0.8
−0.6
−0.4
−0.2
0
(b) SPATIAL SCALE: scaled DAI35
NADA:
mv−Ba:
CAM5−mv−Ba:
LME:
LIM:
Cumulative density function
1
0.9
0.8
0.7
0.6
0.5
0.4
0.3
0.2
0.1
0
−100
−80
−60
−40
−20
0
scaled DAI35

Figure 10: Probability density function (PDF) of the megadrought magnitude (a) and cumulative density function (CDF) of megadrought spatial scale (b). The magnitude parameter is defined by the minimum of the Palmer Drought Severity Index (PDSI), running-mean average over 35 years, PDSI35, over the Southwestern US, SWUS (124°-105°W and 32°-41°N). The spatial scale parameter is defined by the scaled Drought Area Index, scaled-DAI35. The three colored marks are the PDSI35 magnitude and DAI35 spatial scale computed with three different databases: NADA, mv-Ba, and CAM5-mv-Ba; all with a 1000-year record length. The big red dots are the PDSI35 magnitude and DAI35 spatial scale computed with 35 simulations from the Last Millennium Ensemble (LME experiment). Each red dot represents one simulation, so they are plotted using a histogram style. The cyan-colored histograms (PDF and CDF) are computed over a sample time series of 1000-year length with a total pooled of 1000 samples. The primary sample pool is from the 1000-year CAM5-mv-Ba control run. The secondary sample pools were generated by resampling it 1000 times with a 100-year time series of both the PDSI and SST from this CAM5-mv-Ba run, and then using the LIM to stochastically generate a 1000-year new randomized PDSI35 (Ault et al., 2018).